Enhancement of metallic behavior in bismuth cobaltates through lead doping

S. M. Loureiro,* D. P. Young, and R. J. Cava
Department of Chemistry and Materials Institute, Princeton University, Princeton, New Jersey 08544

R. Jin and Y. Liu
Department of Physics, The Pennsylvania State University, University Park, Pennsylvania 16802

P. Bordet
Laboratoire de Cristallographie, CNRS, Boîte Postale 166, 38042 Grenoble Cedex 09, France

Y. Qin and H. Zandbergen
Delft University of Technology, Laboratory for Material Science, 2628 Al Delft, The Netherlands

M. Godinho
Departamento de Física, FCUL, Edifício C1, Campo Grande, 1700 Lisboa, Portugal

M. Núñez-Regueiro
CRTBT, Boîte Postale 166, 38042 Grenoble Cedex 09, France

B. Batlogg
Bell Laboratories, Lucent Technologies, Murray Hill, New Jersey 07974

(Received 22 February 2000; revised manuscript received 23 October 2000; published 30 January 2001)

Single crystals of $Bi_2M_3Co_2O_y$ phases with $M=$Ca, Sr, and Ba were synthesized by the flux method. The undoped Ca and Sr analogs are semiconducting while the Ba analog has a metal to semiconductor transition at $\approx$80 K. Pb-substituted single crystals in which Pb partially substitutes for Bi were prepared by a similar method. Transmission electron microscopy carried out on single crystals of the undoped phases reveals a superstructure similar to that of superconducting bismuth-2212. This superstructure disappears when the Sr and Ba compounds are Pb doped. Transport measurements show that Pb doping induces a clear increase in the metallic character of the samples for Sr and Ba analogs. The metal to semiconductor transition in $Bi_2Ba_3Co_2O_y$ is suppressed by Pb doping, and $(Bi,Pb)_2Ba_3Co_2O_y$ is metallic down to 30 mK. The magnetic-susceptibility data do not show any evidence of ordering, and the magnetic moment Co atom was found to be $\approx 1\mu_B$. Resistivity measurements carried out up to 20 GPa show that the samples become more semiconducting with increasing pressure.

DOI: 10.1103/PhysRevB.63.094109 PACS number(s): 61.14.−x, 75.20.Hr, 81.05.Zx

I. INTRODUCTION

Even though the superconducting cuprates can be formed from a large variety of elements, and crystallize in different structure types, they share several commonalties. These include the same basic functional charge reservoir and conducting blocks, the presence of the (CuO_2) planes where superconductivity is thought to occur, highly hybridized Cu $3d-$O $2p$ bands at the Fermi level, and the appearance of superconductivity where the antiferromagnetic-insulator to paramagnetic-metal transition occurs. Furthermore, in cuprates, Cu^{2+} has a d^9 electronic configuration with the t_{2g} level completely filled. Due to reduced repulsion in the z direction, the d_{z^2} orbital is lower in energy and thus the ninth electron occupies the $d_{x^2-y^2}$ orbital, which is half-filled, a fact that is considered important for the appearance of superconductivity.[1]

Until now, high-T_c superconductivity in nonconventional copper-free systems has been reported in only a handful of compounds. Among these, the chalcogenide ''Chevrel'' phases for which $PbMo_2S_4$ has the highest T_c,[2] the spinel $LiTi_2O_4$,[3] the substituted $BaBiO_3$ perovskite,[4,5] and the intercalated C_{60},[6] are probably the most widely known. In order to investigate whether superconductivity can occur in other noncopper-based systems having half-filled e_g level d bands, we have studied compounds of the $Bi_2M_3Co_2O_y$ $(y=9)$ type. Although the hybridization between Co and O is expected to be different from that displayed by Cu and O, the details of the exact band structure of these compounds are expected to be strongly structure dependent. This suggests that detailed investigation of Co-based materials is necessary in order to determine whether superconductivity can occur only for specific cases. The studied phases are analogous to the known cuprate superconductor $Bi_2Sr_2CaCu_2O_y$ with (Bi_2O_2) layers separated by alternating rocksalt (MO) layers (M being an alkali-earth cation) and (CoO_2) planes.[7] The Bi_2O_2 double layers act as a charge reservoir as in the Bi-2212 superconducting cuprates. The two main differences between the cuprates and cobaltates reside in the fact that (CoO_2) planes replace the (CuO_2) planes, and that in the cobaltates the same alkali-earth cation occupies two different

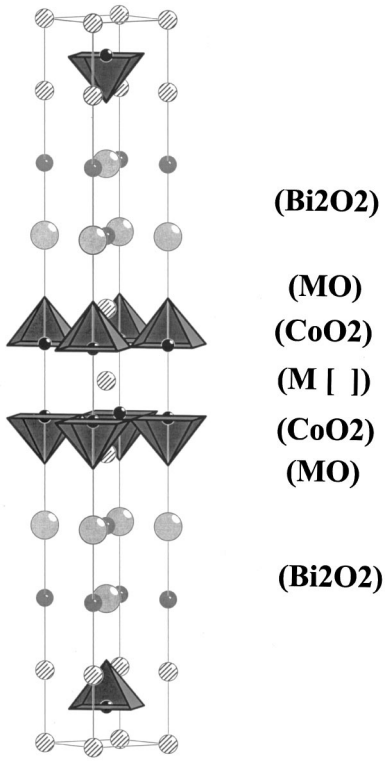

FIG. 1. Structural model of the $Bi_2M_3Co_2O_y$ phase.

positions in the structure. A structural model of $Bi_2M_3Co_2O_y$ is shown in Fig. 1.

These compounds are part of a larger homologous series of general formula $Bi_2M_{n+1}Co_nO_y$ for which several studies have already been reported.[8–15] An x-ray photoelectron spectroscopy study has shown that cobalt has a mixed valence state $(2+, 3+)$ for $n=1$, and is $(3+)$ when $n=2$.[8] This study also showed that the first members are antiferromagnetic insulators with $T_N = 100-250$ K.[9] The ac susceptibility data for the second member of the series showed that the Curie constant C is small and independent of the direction of the field, suggesting that Co^{3+} is in the d^5 low-spin configuration. The metallic character increases with both, the number of (CoO_2) layers and the size of the M alkali-earth cation. Infrared-reflectivity measurements have also confirmed this fact.[10] Attempts to change the oxygen content did not induce superconductivity.[8]

II. EXPERIMENT

Single crystals of $(Bi_{1-x}Pb_x)_2M_3Co_2O_y$ (M = Ca, Sr, and Ba) were prepared using a mixture of Bi_2O_3, PbO, MCO_3, and Co_3O_4 in the temperature range 1100–1230 °C with different cooling rates (6–8 °C/h) under air. A mixture of Bi_2O_3/Co_3O_4 was used as flux. The ratio PbO/Bi_2O_3 was varied and increased up to 1:1 in weight (w/w). Using this method, large platelike single crystals up to 10 mm in length were synthesized. The crystals were formed as numerous micrometer-thin plates with striations. As for the Bi-2212 superconducting analogs, they are extremely cleavable and were easily removable from the crucibles with tweezers. Flux sometimes adhered to the surface, especially when the samples were heavily Pb doped. For brevity, the following nomenclature will refer to the sample compositions [the suffixes 0, 1/3, and 1/1 indicate Pb free, $PbO/Bi_2O_3 = 1/3$ (w/w), and $PbO/Bi_2O_3 = 1/1$ (w/w), respectively]:

$$\text{CaPb0}=[Bi_2Ca_3Co_2O_y],\quad \text{CaPb1/3}=[(Bi,Pb)_2Ca_3Co_2O_y],\quad \text{CaPb1/1}=[(Bi,Pb)_2Ca_3Co_2O_y],$$

$$\text{SrPb0}=[Bi_2Sr_3Co_2O_y],\quad \text{SrPb1/3}=[(Bi,Pb)_2Sr_3Co_2O_y],\quad \text{SrPb1/1}=[Bi,Pb)_2Sr_3Co_2O_y],$$

$$\text{BaPb0}=[Bi_2Ba_3Co_2O_y],\quad \text{BaPb1/3}=[(Bi,Pb)_2Ba_yCo_2O_y],\quad \text{BaPb1/1}=[(Bi,Pb_2Ba_3Co_2O_y].$$

Powder samples of the Ca and Sr analogs were also prepared by solid-state reactions from similar starting materials at 800 °C for 144 h, with several intermediate grindings.

X-ray powder diffraction was carried out using a Rigaku Miniflex powder diffractometer with Cu $K\alpha$ radiation ($\lambda = 1.540\,56$ Å) at room temperature. The transmission electron microscopy (TEM) measurements were carried out on several crystallites of the samples using a Philips CM30T electron microscope operating at 300 kV. The magnetic measurements were carried out on batches of randomly oriented crystals of samples CaPb0, CaPb1/1, SrPb0, SrPb1/1, BaPb0, and BaPb1/1 using a superconducting quantum interference device dc magnetometer operating at 1 T. The normal-state transport measurements were carried out on single crystals of Pb-free and heavily Pb-doped Ca, Sr, and Ba analogs with a standard four-probe technique, in a temperature range between 5 and 300 K using the transport option of a physical property measuring system by Quantum Design. Typical dimensions of the selected samples were about $1.0\times0.5\times0.1$ mm^3. For each sample, two current and two point-shaped voltage contacts were positioned so that the applied dc current flowed in only one crystallographic direction.

The electrical resistivity measurements under high pressure were performed in a sintered diamond Bridgman anvil apparatus using a pyrophillite gasket and two steatite disks as the pressure medium. The two platelike samples employed, of size $0.2\times0.03\times0.05$ mm^3, were obtained by cleaving one crystal. The Cu-Be device that locks the anvils can be cycled between 1.2 and 300 K in a sealed Dewar. Pressure was calibrated against the phase transitions of Bi under pressure at room temperature and by the superconductivity transition of a Pb manometer at low temperature. The overall uncer-

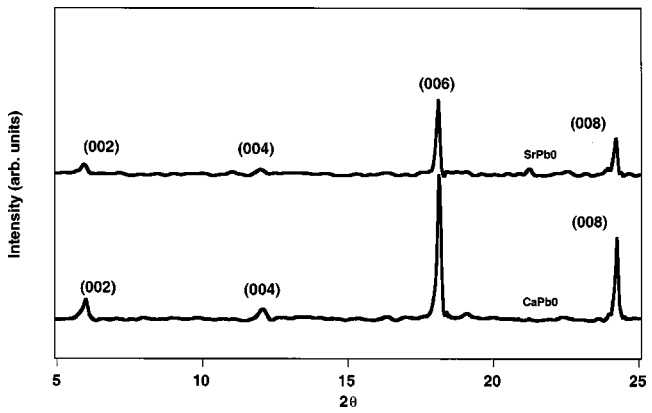

FIG. 2. X-ray powder diffraction of samples CaPb0 $[Bi_2Ca_3CoO_y]$ and SrPb0 $[Bi_2Sr_3CoO_y]$ in the 2θ region 5°–25°, showing strong preferred orientation in the 00l direction.

tainty in the quasihydrostatic pressure is estimated to be $\pm 10\%$. The pressure spread across the sintered diamond anvils was determined on Pb manometers to be ≈ 1.5–2 GPa depending on the applied pressure. The temperature was measured using a calibrated carbon glass thermometer with a maximum uncertainty (mainly due to temperature gradients across the Cu-Be clamp) of ≈ 0.5 K. Four-probe electrical resistivity dc measurements using platinum leads were made with a Keithley 182 nanovoltmeter combined with a Keithley 238 current source. The Seebeck coefficient was measured between 200–500 K using a commercial microminiature refrigerators (MMR) technology apparatus.

III. RESULTS

A. Synthesis and crystal structure data

The x-ray patterns of the powder Ca and Sr analog samples show that the $Bi_2M_3Co_2O_y$ phase was present as the major component, even though several impurity phases were also detected. The patterns reflect the preferred orientation of platelike crystals since most reflections belonged to the 00l family. Figure 2 shows the low-angle portion of the powder pattern that allowed a correct identification of the stacking of the phases and a good accuracy in the determination of the c axis. Due to the presence of impurities, a and b axes are affected by overlapping reflections. Both Pb-free Ca and Sr analogs could be indexed in an average tetragonal cell with lattice parameters $a=b=5.033(3)$ Å, $c=28.52(8)$ Å, and $a=b=5.012(3)$ Å, $c=29.09(3)$ Å, respectively. In agreement with previous reports,[8] it was not possible to prepare powder samples of the Ba analog.

Due to the extreme layered nature of these compounds and their inelastic bending properties, crystal-structure determination by single-crystal x-ray diffraction has never been reported. Tarascon *et al.* reported crystal data based on selected-area electron diffraction on crystallites of the $Bi_aM_{n+1}Co_zO_y$ phases.[8] The Ca analog was orthorhombic with lattice parameters $a=4.89$ Å, $b=5.06$ Å, and an incommensurate modulation of 28.4 Å along a. The Sr analog possessed two modulations, one commensurate with reciprocal periodicity given by $(3a^*+b^*)/18$ and one incommensurate given by $(a^*/11.3)$. A modulation along [110] was found for the Ba analog. Both Sr and Ba analog exhibited deviation from orthorhombic symmetry in the [001] zone axis.

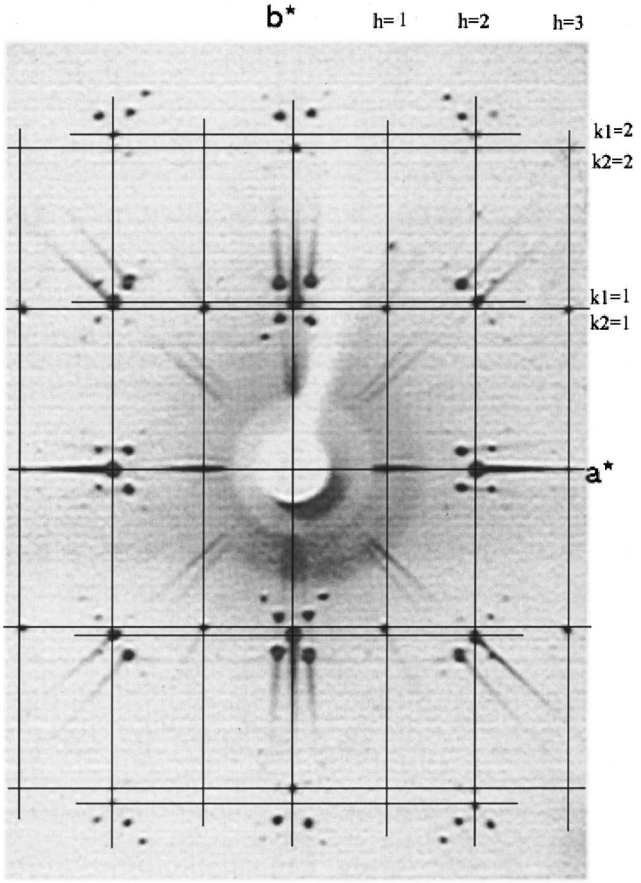

FIG. 3. X-ray diffraction precession image of the $(hk0)$ plane of a Pb-free Sr analog SrPb0 single crystal.

Some of the synthesized crystals were selected and examined by the precession technique, using Zr-filtered Mo K_α radiation. For almost all of the analyzed specimens, it was not possible to collect good diffraction patterns due to the complex nature of the crystals. Furthermore, most of the thin-plate crystals were bent and thus displayed poor diffraction patterns. Only for the SrPb0 batch were we able to collect meaningful $(hk0)$ diffraction patterns. The x-ray diffraction precession image of the analyzed SrPb0 crystal is shown in Fig. 3.

Two distinct sublattices are required to index the diffraction indicating that this material must have a ''misfit'' structure.[16] (A ''misfit'' structure can arise in layered compounds when the periodicities of two or more layers are incommensurate, and the bonding between layers is weak relative to bonding within the layers.) The two sublattices are indicated in the figure. The first sublattice has cell parameters $a_1=4.94$ Å and $b_1=2.68$ Å. Although diffraction spots were markedly elongated due to crystal bending, the $(h0l)$ diffraction plane indicated monoclinic symmetry with $c_1=29.9$ Å, and $\beta_1=95°$. The main diffraction spots in the $(hk0)$ plane are surrounded by superlattice peaks that can be

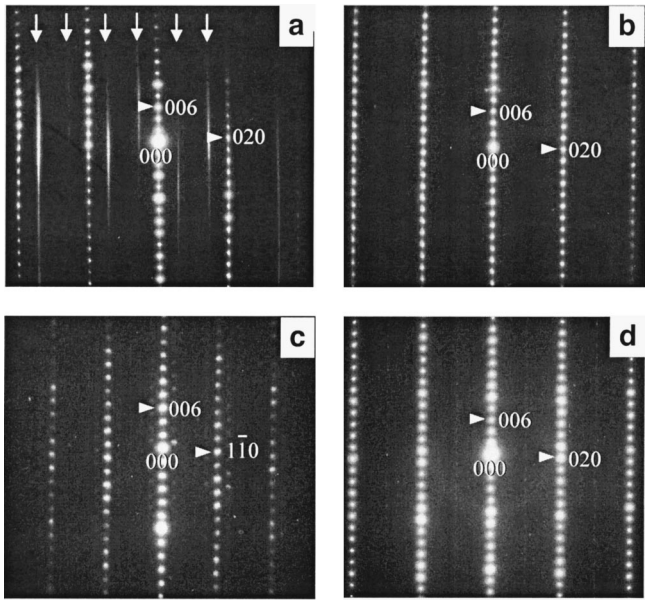

FIG. 4. Electron diffraction in the [100] zone axis for samples CaPb1/3 (a), SrPb1/1 (b), and BaPb1/1 (d), and [110] zone axis of BaPb0 (c).

indexed with the incommensurate modulation vector $q^* = 0.17a_1^* + 0.056b_1^*$. This modulation is quite strong and satellite peaks up to the third order can be observed. The second sublattice, having somewhat weaker intensity, can be indexed with $a_2 = a_1$, $b_2 = 2.79$ Å, $c_2 = c_1$, $\beta_2 = \beta_1$.

B. Transmission electron microscopy

The lattice parameters found by TEM for some of the samples studied were consistent with the values expected for a $Bi_2M_3Co_2O_y$ type of phase. The *a* and *b* axes remain fairly constant at ≈5.0 Å for all analogs, while the *c* axis increases consistently with the increase in the atomic radius of the alkali-earth cation, from 30.5 Å for Ca, to 30.8 Å for Sr, to 31.8 Å for Ba. They are nearly indistinguishable between Pb-free and Pb-doped compounds. To ensure that Pb was incorporated into the phases, we carried out energy dispersive spectroscopy analysis on several crystallites of the SrPb1/1 and BaPb1/1 samples. This yielded $(Bi_{0.55}Pb_{0.45})_2(Bi_{0.15}Sr_{0.85})_3Co_2O_y$ for the Sr analog, and $(Bi_{0.7}Pb_{0.3})_2(Bi_{0.2}Ba_{0.8})_3Co_2O_y$ for the Ba analog, showing that in the phases, lead substitutes for bismuth and bismuth substitutes for barium or strontium.

The TEM results showed that in the Ca-analog samples, the Br-2212 superstructure type is present in both Pb-free and Pb-doped samples. However, in samples of Sr and Ba analogs, only the Pb-free samples present the superstructure. Figure 4 shows the [100] zone-axis electron-diffraction pattern of samples CaPb1/3 (a), SrPb1/1 (b), and BaPb1/1 (d) as well as the [110] zone axis of BaPb0 (c). The electron-diffraction patterns are indexed relative to a tetragonal-type cell. The arrows indicate the presence of diffuse streaks in the electron-diffraction pattern of CaPb1/3.

C. Magnetic measurements

The temperature dependence of the inverse magnetic susceptibility for batches of randomly oriented single crystals is linear and shown in Fig. 5. The magnetic moment per Co atom is fairly constant, independent of alkali-earth or Pb content, and $\approx 1\mu_B$/Co atom. For the Pb-free samples, the data showed $0.80\mu_B$ for CaPb0, $0.84\mu_B$ for SrPb0, and $0.85\mu_B$ for BaPb0. These increase for heavily Pb-doped samples, being $1.35\mu_B$ for CaPb1/1, $0.98\mu_B$ for SrPb1/1, and $0.96\mu_B$ for BaPb1/1. Figure 6 shows the temperature dependence of the inverse magnetic susceptibility along the crystallographic axes of a single crystal of BaPb1/1. The crystallographic axes were assigned taking into account the striations of the crystal. A direction parallel to the striation indicates the *a* axis, perpendicular to the striation indicates the *b* axis and in-plane perpendicular to the striation indicates the *c* axis. The inverse magnetic susceptibility as a function of temperature is once more linear and the effective moment/Co atom is near $1\mu_B$; being $1.11\mu_B$ along *a*, $0.94\mu_B$ along *b*, and $1.07\mu_B$ along *c*. No indication of long-range ordering was found down to 2 K.

D. Transport properties

The normalized resistance for single crystals of the Ca analogus as a function of the temperature is shown in Fig. 7.

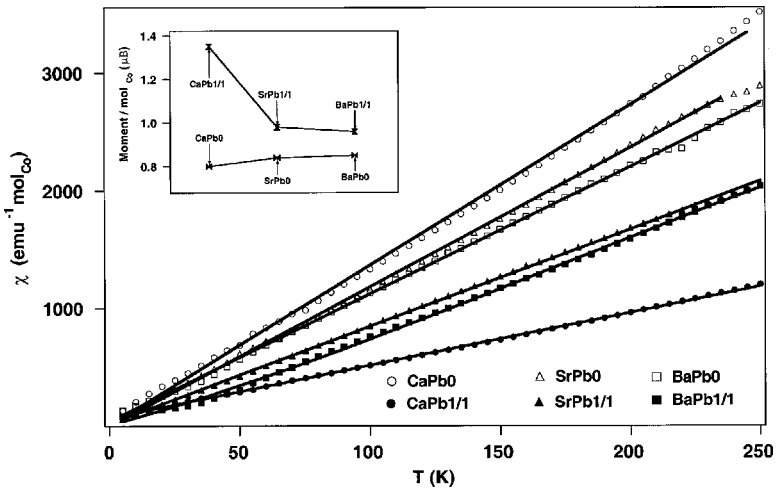

FIG. 5. Temperature dependence of the inverse magnetic susceptibility for samples CaPb0, CaPb1/1, SrPb0, SrPb1/1, BaPb0, and BaPb1/1. The inset represents the obtained magnetic moment/mol Co atom of Pb-doped and Pb-free samples plotted against the ionic radius of *M* in coordination number 8.

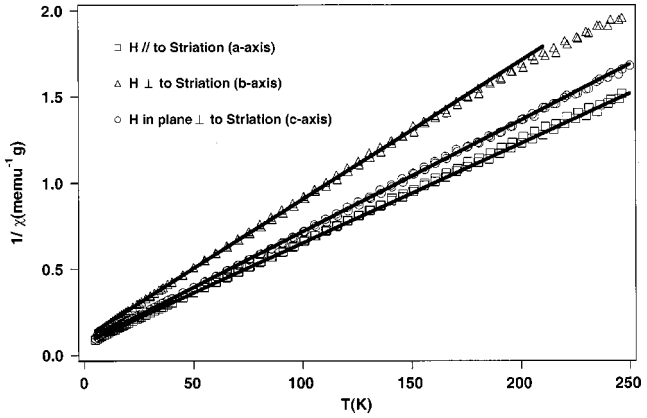

FIG. 6. Temperature dependence of the inverse magnetic susceptibility for a single crystal of heavily Pb-doped Ba analog BaPb1/1 along the crystallographic directions of the crystals.

These samples (CaPb0, CaPb1/3, and CaPb1/1) were always semiconducting, even for heavily Pb-doped samples. The Ca analogs seem to present an interesting case since they show a different trend when compared to the Sr and Ba analogs. They become more semiconducting on increasing Pb substitution and show activated behavior in a 100-K range (between ≈50–150 K). The activation energy increases with the level of Pb substitution: ≈0.26 eV for CaPb0, ≈0.34 eV for CaPb1/3, and ≈0.37 eV for CaPb1/1. Attempts to fit the data according to two-dimensional (2D) or 3D VRH (variable-range hopping) models were unsuccessful.

The Sr analog substantially change their behavior when Pb-doped (Fig. 8). Sample SrPb0 displays typical semiconducting behavior, while SrPb1/3 shows a metal to semiconductor transition at ≈80 K. In SrPb1/1, the heavily Pb-doped sample, the metal to semiconductor transition is shifted to even lower temperatures, 30 K, a behavior only displayed by some Ba-bearing analogs. The Pb-free Ba analog (BaPb0) shows a metal to semiconductor transition at 80 K (Fig. 9). Similar behavior has been previously reported.[7] For Pb-doped samples (BaPb1/3), the transition is dramatically shifted to 10 K, approximately 70 K below the Pb-free sample value, and the sample is almost completely metallic.

Taking this trend into account, we proceeded to a careful examination of the resistivity of the heavily Pb-doped samples, BaPb1/1. Figure 10 shows the typical temperature dependence of the electrical resistivity for each crystallographic direction of two crystals of BaPb1/1. For the most part, the resistivities decrease with decreasing temperature without any particular feature down to 10 K. As the temperature is further lowered, the resistivities reveal a sharp decrease for crystal 1 suggesting that a transition occurs around 5–10 K. The resistivity in each direction remains nonzero at the lowest temperature measured. An explanation for this result is that crystal 1 has a superconducting BaPbBiO phase embedded in its matrix. Superconductivity has been observed in the $BaPb_{1-x}Bi_2O_3$ system with transition temperature $T_c \sim 10\,\mathrm{K}$.[4] This phase is formed in growing $(Bi, Pb)_2Ba_3Co_2O_y$ and was detected by x-ray powder diffraction in the flux. However, the properties displayed by crystal 2 are far more representative of the majority of the crystals we have obtained. Although determining the origin of this resistance drop requires further work, we believe that the observed metallic behavior in the resistivity represents an intrinsic property of this material. A single crystal of BaPb1/1 was tested down to 30 mK in order to check for zero resistance at very low temperatures. Superconductivity, however, was not observed.

In order to check for the dominant transport mechanism, we carried out measurements of the Seebeck coefficient in the range 200–500 K along the *b* axis. Figure 11 shows that the Seebeck coefficient is positive, thus, the majority of carriers along the transition-metal oxide planes seem to be holes.

E. Resistivity under high pressure

Volume compression by pressure can be used as a tunable probe to test properties of materials. It can induce variations of the structural parameters responsible for the studied properties. Compared to chemical substitutions, where several parameters are changed simultaneously and other undesirable ''side effects'' may occur, the application of pressure can produce a relatively ''clean'' variation. In particular, it has been found in high-temperature superconducting cuprates that application of pressure resulted in an increase of the carrier concentration, as monitored by Hall-effect

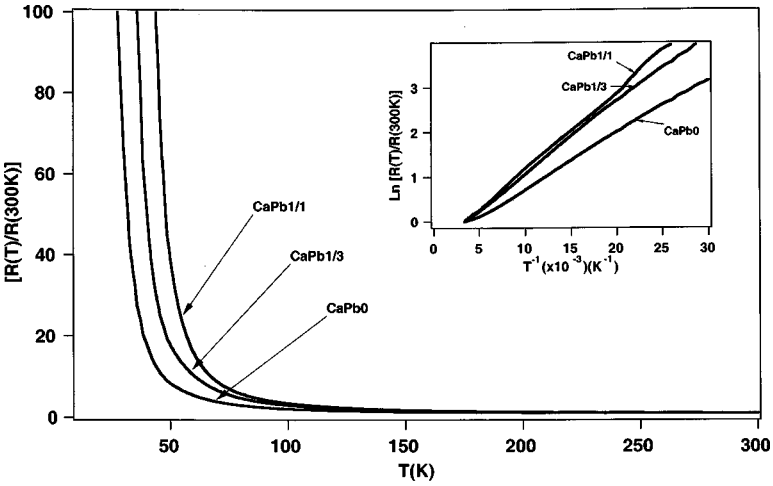

FIG. 7. Normalized resistance measurements carried out on single crystals of samples CaPb0, CaPb1/3, and CaPb1/1. The inset represents plots of the logarithm of the normalized resistance as a function of the inverse temperature.

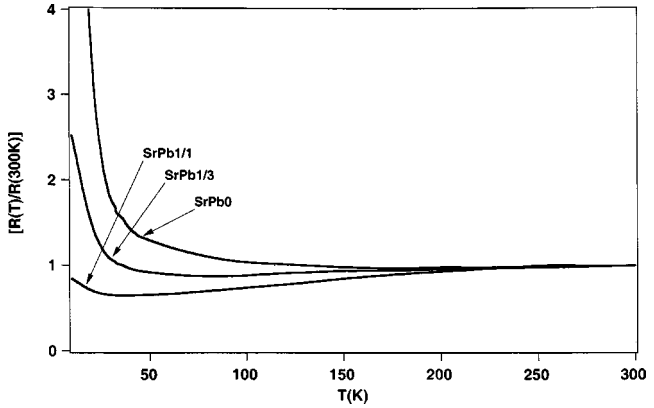

FIG. 8. Normalized resistance measurements carried out on single crystals of samples SrPb0, SrPb1/3, and SrPb1/1.

measurements.[14] To test if similar effects could be obtained on cobaltates, sample BaPb1/1 was measured under high pressure.

The logarithm of the resistance of a single crystal of BaPb1/1 is plotted vs $T^{-1/4}$ in Fig. 12. The resistance is observed to increase with pressure. The dominant transport mechanism is 3D VRH. Such behavior exists even for the lowest applied pressure, 2.5 GPa. As seen in the resistance measurements at normal pressure, the behavior observed under high pressure is consistent with the fact that smaller alkaline-earth cations are more semiconducting.

IV. DISCUSSION

The main difference between the Bi-2212 superconductors and the Bi-cobaltates [other than the obvious presence of (CoO_2) planes] resides in the fact that in the latter, the same type of alkali-earth atom is present in two different sites (M_I and M_{II}), adopting two different types of coordination. In the (MO) layer, M_I is coordinated to four coplanar oxygen atoms, four additional oxygen atoms in the (CoO_2) plane below, and one Bi atom in the plane above. In the $(M[\,])$ layer ([ ] indicates vacancy), M_{II} is coordinated to eight oxygen atoms, four above and four below in the (CoO_2) planes.

Several reasons may account for the differences in behavior displayed by the M analogs and their substitutions. The Pb atom in octahedral coordination has ionic radii of 1.19 and 0.775 Å for oxidation states Pb^{2+} and Pb^{4+}, respectively. Taking into account the very small value of the ionic radius of Pb^{4+}, we can surmise that lead is more likely to be in the oxidation state $2+$ in the present compounds, and thus act as a hole dopant. This is corroborated by the fact that Pb-doped samples of the Sr analog display similar results as those of thin-film undoped samples grown under ozone atmosphere, which have a much higher oxygen content (oxygen intercalation is another form of hole doping).[13] The Seebeck coefficient measured between 200–500 K was positive and confirmed our supposition that the carriers are indeed holes. In any case, either due to oxygen intercalation in the form of O_δ or due to lead doping, the oxidation state of cobalt should be $3+$ or higher.

Even though several models have been proposed to explain the origin of the superstructure modulation in bismuth superconductors, there is still no final consensus on the exact

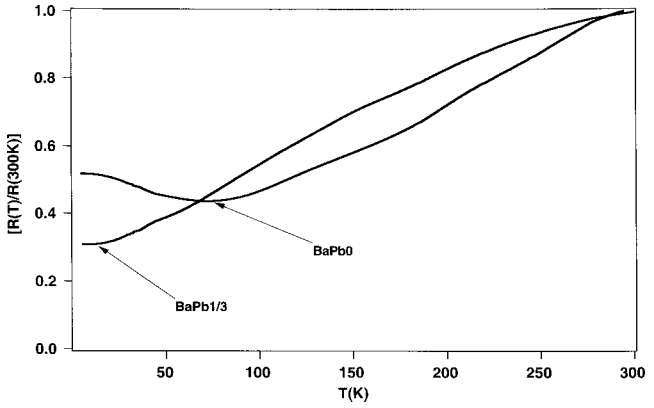

FIG. 9. Normalized resistance measurements carried out on single crystals of samples BaPb0 and BaPb1/3.

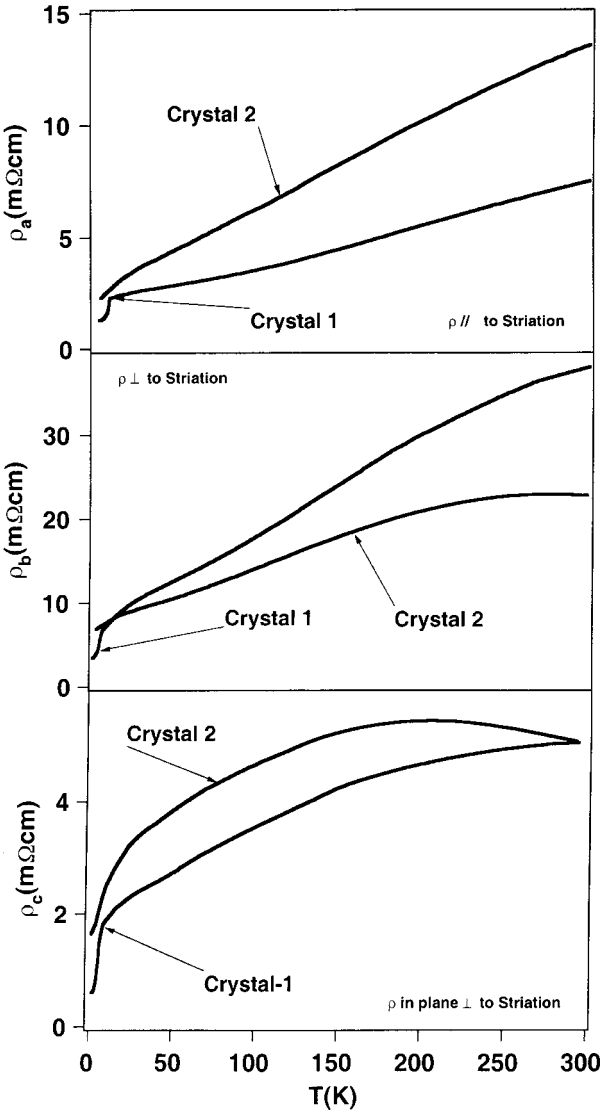

FIG. 10. Temperature dependence on the resistivity for two different single crystals of BaPb1/1.

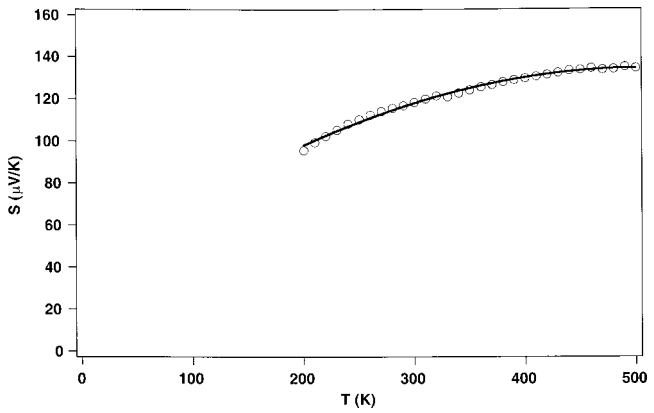

FIG. 11. Seebeck coefficient of a single crystal of BaPb1/1 measured between 200–500 K.

answer for this complex problem.[7,17,18] One of these models suggests that the origin of the structure in Bi-2212 is due to periodic contraction/expansion of the slabs caused by oxygen intercalation.[7] In this series, Ca analogs show the superstructure in both Pb-free and Pb-doped compositions, while Sr and Ba analogs only show it for Pb-free samples. When Pb^{2+} is introduced in the structure, it replaces Bi^{3+}, which is smaller in ionic radius by some 0.16 Å. This may cause stress in the adjacent (M_1O) layers as well as in the (CoO_2) planes, since these are, in their turn, constrained by the same type of cation with lower ionic radius due to lower coordination. Lead substitution may indeed randomize the periodicity of inclusion of oxygen into the (Bi_2O_2) slab. The fact that Ca samples present the superstructure even when Pb doped may relate to the fact that calcium in the adjacent layer has an ionic radius intermediate between that of lead (1.19 Å) and bismuth (1.03 Å) (but in any case smaller than lead), and that both Sr and Ba analogs have ionic radii bigger than lead. [The alkali metals in the oxidation state 2+ have the following ionic radii for their respective coordination (M^{2+} in coordination number 8 and 9): Ca^{2+} = 1.12/1.18 Å, Sr^{2+} = 1.26/1.32 Å, and Ba^{2+} = 1.42/1.47 Å].

The bismuth cobaltates in the undoped state (Pb-free, O_δ=0) should have cobalt in the oxidation state 3+ with low-spin electronic configuration, and thus should not show magnetic moment. However, we found experimental evidence of $\approx 1\,\mu_B$/mol cobalt in our samples. The obtained moment is smaller than the one expected for atoms with one unpaired electron ($1.73\,\mu_B$), but still not negligible. Two possibilities may account for the moment found in these compounds. The first relates to a change in electronic configuration of Co due to hole doping caused by oxygen intercalation or lead doping. This is corroborated by the fact that the moments increase for lead-doped phases independently of the *M* cation considered. The smaller than expected moment may simply reflect the average spin state of the cobalt atoms in the samples. Some cobalt atoms may indeed have one unpaired electron while in others this effect is diluted due to charge-transfer mechanisms within the covalent *M*-O bond. The second possibility may relate to structural reasons. A smaller cation like calcium may cause a contraction of the (CoO_2)(Ca[ ])(CoO_2) cage and a better coupling between planes, thus a greater interaction between the moments. As observed through the magnetic measurements carried out on these phases, the obtained magnetic moment is indeed larger for smaller *M* cations.

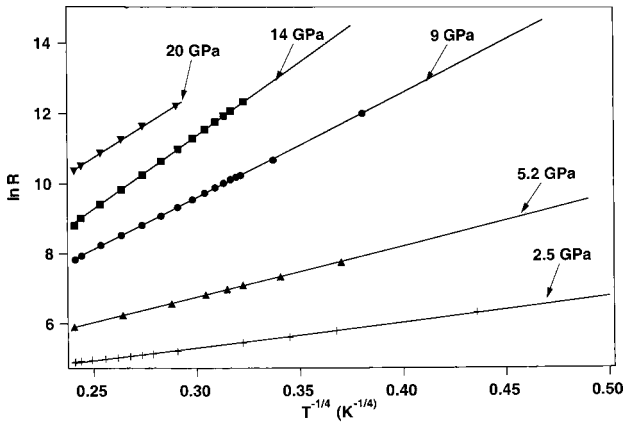

FIG. 12. Pressure dependence of the resistivity of a single crystal of BaPb1/1, showing 3D VRH behavior.

The normal-state resistivity data for the Sr and Ba analogs shows a clear increase of metallic character with increase in ionic radius in the alkali-earth cation, in agreement with the results reported by Tarascon *et al.*[3] The Ba analogs were known to display the metal to semiconductor transition near 80 K. High-oxygen pressure treatment of samples carried out by the same authors did not seem to significantly change the transport properties of the compound. However, when one introduces an ''internal'' dopant into the structure such as Pb, the transport properties change significantly. For the Sr analogs, the sample SrPb0 was a semiconductor over the measured temperature range, but the material became metallic down to 80 K when Pb doped, in agreement with Hervieu *et al.*,[16] who reported similar results for Pb-doped BiSrCoO oxides that crystallize in a misfit structure type. Increasing Pb substitution shifts the metal to semiconductor transition downward to 30 K. The same behavior can be obtained only when undoped Sr analogs are prepared using a clean thin-film technique in an oxygen-rich atmosphere (ozone).[13] This would corroborate the fact that Pb would be acting as a hole dopant in this system. The clearest effect is shown by the Ba analogs where the intermediately doped sample BaPb1/3 and the heavily doped sample BaPb1/1 became metallic down to 7 K and 30 mK respectively.

The resistivities of these materials increase under pressure. From the pressure-dependent resistivity data displayed in Fig. 13, where the behavior is well described by 3D-VRH($\rho \approx \rho_0 \exp(T_0/T)^{1/4}$), $1/T_0$ is plotted vs pressure. If we consider that we are dealing with carrier localization by disorder, it can be shown that $1/T_0 \approx \kappa_B N(\varepsilon_F)/\alpha^3$, where k_B is the Boltzmann constant, α is the localization distance, and $N(\varepsilon_F)$ is the density of states at the Fermi level ε_F.[19] As we do not expect the localization distance to change with pressure (this is generally caused by impurities, whose number does not change with pressure), we can ascribe the variation of $T_0[N(\varepsilon_F)]$ to a measure of the occupied states. It is clear

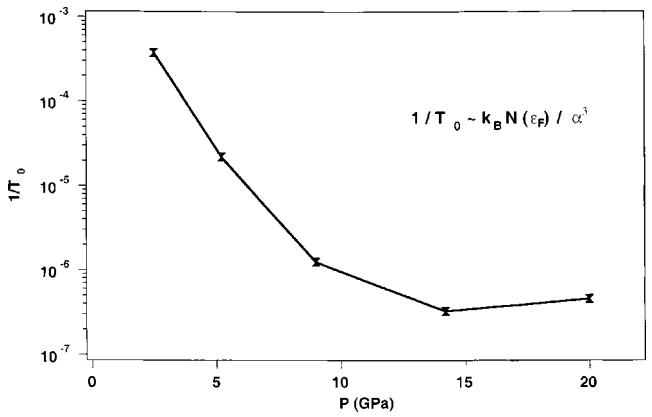

FIG. 13. Pressure dependence of the number of carriers for single crystals of BaPb1/1 samples.

that for single crystals of sample BaPb1/1 the number of carriers decreases with pressure. This is consistent with the trend displayed by the series when M is smaller, and is consistent with the data obtained for the Ca analogs at ambient pressure. When submitting Sr or Ba analog to pressure, we are mimicking the effect of substitution for a smaller cation such as calcium, i.e., physical pressure becomes equivalent to chemical pressure.

Usually for cuprates, and similar-layered materials with active and reservoir layers, pressure reduces the ionicity of the layers as the interplanar distances decrease.[20] This implies a charge (hole) transfer from the reservoir layers to the active CoO_2 layers. However, due to the complexity of these materials, other effects like partial substitution of Bi for the alkali-earth cation or an increase of corrugation of the CoO_2 planes may occur. This will effectively reduce the mobility or the carrier density in the planes and can in fact act as the predominant factor. Our results can be explained in these last terms (corrugation of the CoO_2 planes), and are also consistent with the chemical pressure introduced by Sr and Ca replacement.

V. CONCLUSIONS

The goal of this study was to search for superconducting systems that might provide some insight as to why cuprates superconduct. The bismuth cobaltates present a good opportunity for comparing local environments of transition-metal–oxygen planes in layered cobalt and copper oxides. For this purpose, a series of single crystals of compounds with general formula $(Bi, Pb)_2M_3Co_2O_y$ (M=Ca, Sr, and Ba) was prepared by the flux method and structural data of this type of compound were collected by single-crystal x-ray diffraction. The analyzed single crystal of nominal composition $Bi_2Sr_yCo_2O_y$ was found to crystallize in a misfit structure of monoclinic symmetry with lattice parameters related by two sublattices with $a_1=4.94$ Å, $b_1=2.68$ Å, $c_1=29.9$ Å, $\beta_1=95°$, and incommensurate modulation vector $q^*=0.17a_1^*+0.056b_1^*$, and $a_2=a_1$, $b_2=2.79$ Å, $c_2=c_1$, $\beta_2=\beta_1$, respectively (however, since this was for a single specimen analyzed, it is not impossible to generalize the misfit type of structure of the series of $Bi_2M_3Co_2O_y$ compounds).

The relative differences in the ionic radii of the various M^{2+} in coordination 9 and Pb^{2+} may explain why the superstructure is destroyed when the compounds are Pb doped for Sr and Ba analogs, and remains intact for any composition of the Ca analog. The Pb doping effectively changes the transport properties of the compounds rendering them fully metallic. At the present stage, the compounds are not superconducting.

An angle-resolved photoelectron spectroscopy study on these compounds is currently underway. This will supply further insight about their electronic structure and will possibly allow a direct comparison with the superconducting cuprates. It may also suggest new doping routes and how to achieve superconductivity in these type of phases.

ACKNOWLEDGMENTS

This research was funded by the Department of Energy, Grant No. DE-FG02-98-ER45706. S.M.L. wishes to thank INICT/PRAXIS XX/BPD18834/98.

*FAX: (609) 258 6746. E-mail address: loureiro@princeton.edu

[1] R. J. Cava, J. Am. Ceram. Soc. **83**, 5 (2000), and references therein.

[2] B. T. Mathias, M. Marezio, H. E. Barz, E. Corenzwit, and A. S. Cooper, Science **175**, 1465 (1972).

[3] D. C. Johnston, H. Prakash, W. H. Zandbergen, and R. Viswanathan, Mater. Res. Bull. **8**, 777 (1973).

[4] A. W. Sleight, J. L. Gillson, and P. E. Bierstedt, Solid State Commun. **17**, 27 (1975).

[5] R. J. Cava, B. Batlogg, G. P. Espinoza, A. P. Ramirez, J. Krajewski, W. F. Peck, Jr., L. W. Rupp, and A. S. Cooper, Nature (London) **339**, 291 (1989).

[6] T. T. M. Palstra, O. Zhou, Y. Iwasa, P. E. Sulewski, R. M. Fleming, and B. R. Zegarsig, Solid State Commun. **93**, 327 (1995).

[7] Y. LePage, W. R. McKinon, J.-M. Tarascon, and P. Barboux, Phys. Rev. B **40**, 6810 (1989).

[8] J.-M. Tarascon, R. Ramesh, P. Barboux, M. S. Hedge, G. W. Hull, L. H. Greene, M. Giroux, Y. LePage, W. R. McKinnon, J. V. Waszcak, and L. F. Schneemeyer, Solid State Commun. **71**, 663 (1989).

[9] J.-M. Tarascon, P. Barboux, G. W. Hull, R. Ramesh, L. H. Greene, M. Giroud, M. S. Hedge, and W. R. McKinnon, Phys. Rev. B **39**, 4316 (1989).

[10] Y. Watanabe, D. C. Tsui, J. T. Birmingham, N. P. Ong, and J.-M. Tarascon, Phys. Rev. B **43**, 3026 (1991).

[11] P. A. Suzuki, R. F. Jardim, and M. C. A. Fantini, Mater. Lett. **12**, 321 (1991).

[12] I. Terasaki, T. Nakahashi, A. Maeda, and K. Uchinokura, Phys. Rev. B **47**, 451 (1993).

[13] C. Murayama, Y. Iye, T. Enomoto, N. Mori, Y. Yamada, T. Matsumoto, Y. Kubo, Y. Shimakawa, and T. Manako, Physica C **183**, 335 (1991); I. Tsukada, M. Nose, and K. Uchinokura, J. Appl. Phys. **80**, 5691 (1996).

[14] I. Tsukada, T. Yamamoto, M. Takagi, T. Tsubone, and K. Uchinokura, in *Science and Technology of Magnetic Oxides*, edited by M. Hundley *et al.*, MRS Symposia Proceedings No. 494 (Materials Research Society, Pittsburgh, 1998), p. 119; I. Tsukada, I. Terasaki, T. Hoshi, F. Yura, and K. Uchinokura, J.

Appl. Phys. **76**, 1317 (1994).
[15] T. Yamamoto, I. Tsukada, and K. Uchinokura, Jpn. J. Appl. Phys., Part 1 **38**, 1949 (1999).
[16] M. Hervieu, Ph. Boullay, C. Michel, A. Maignan, and B. Raveau, J. Solid State Chem. **142**, 305 (1999).
[17] Z. Q. Mao, J. A. Zuo, M. L. Tian, G. J. Xu, C. Y. Xu, Y. Wang, J. S. Zhu, and Y. H. Zhang, Phys. Rev. B **53**, 12 410 (1996).
[18] X. B. Kan and S. C. Moss, Acta Crystallogr., Sect. B: Struct. Sci. **48**, 122 (1992).
[19] N. F. Mott and E. A. Davis, *Electronic Processes in Non-crystalline Materials* (Clarendon, Oxford, 1979).
[20] M. Núñez-Regueiro and C. Acha, *Studies of High-T_c Superconductors* (Nova Science, New York, 1997), Vol. 24, p. 203, and references therein.